Hydrogen Scrambling in $[(C_5Me_5)Os(dmpm)(CH_3)H]^+$. A Density Functional and ONIOM Study

Robert K. Szilagyi, Djamaladdin G. Musaev,* and Keiji Morokuma*

Cherry L. Emerson Center for Scientific Computation and Department of Chemistry, Emory University, Atlanta 30322, Georgia

Received August 27, 2001

The hydrogen scrambling in the "model" compound $[CpOs(PH_2CH_2PH_2)(CH_3)H^*]$ and the experimentally used "real" compound $[Cp^*Os(PMe_2CH_2PMe_2)(CH_3)H^*]^+$ was studied with the density functional (B3LYP) and ONIOM (B3LYP:HF) method, respectively. The solvent effects were taken into account with a polarizable continuum model (PCM). Examination of five postulated mechanisms indicates that the H-scrambling takes place via the H-exchange mechanism. The first step of this reaction is the C−H* bond formation that takes place via a three-centered transition state. The zero-point-corrected barrier of this rate-determining step is 6.0 kcal/mol for the model compound without solvent and is increased to 8.9 kcal/mol in $CHCl_3$ solution and to 8.8 kcal/mol for the real compound without solvent. Overcoming this barrier leads to formation of the methane complex, which can rearrange to its identical isomer with a small barrier (<2 kcal/mol). The isomer now can go through the reverse processes of the above, via methane C−H bond activation with a barrier of 6.2, 6.3, and 2.9 kcal/mol, respectively, leading to the scrambled product. The electronic and steric effects of the nine methyl substituents in the real system are to destabilize the transition states and intermediates by several kcal/mol, to increase the rate-determining C−H* bond formation barrier, and reduce the reverse C−H activation barrier. The associative/dissociative mechanism, proceeding via dissociation of the methane molecule from the methane complex, is found to be only slightly less favorable in free energy and may be competitive.

I. Introduction

Recently the first example of transition metal methyl/hydride complexes, $[(C_5Me_5)Os(dmpm)(CH_3)H]^+$ (dmpm = bis(dimethylphosphino)methane, **I**), has been reported, in which hydrogen atoms of the alkyl and hydride ligands exchange at a rate detectable in the NMR time scale.[1] It has been shown that the hydrogen scrambling occurs with $\Delta H^{\ddagger} = 7.1 \pm 0.9$ kcal/mol, $\Delta S^{\ddagger} = -6.5 \pm 5$ eu, and $\Delta G^{\ddagger} = 8.1$ kcal/mol at −100 °C, 1 atm. The reductive elimination of methane from this complex is said to be a first-order reaction with $\Delta G^{\ddagger} =$ 13.5 kcal/mol at −100 °C, 1 atm, which was attributed to a different transition state.

In the literature, five different mechanisms were proposed for this reaction, as shown in Scheme 1.[1] All pathways start from the complex **I** with a (H*)[Os](CH_3) core and lead to the complex **I′** with a (H)[Os](CH_2H^*) core. Path A is an "oxidative addition" mechanism and starts with oxidative addition of the methyl C−H bond to a metal center leading to formation of (H)(H*)[Os]═CH_2 complex **II**, which later undergoes the reductive elimination to form a C−H* bond and leads to the final product **I′**. Path B, "σ-bond metathesis" mechanism, occurs via the activation of the methyl C−H bond by the σ-bond metathesis mechanism and leads to formation of dihydrogen-methylene intermediate (HH*)[Os]═CH_2, **III**, where the (HH*) molecule rotates and is activated via the same "σ-bond metathesis" transition state, leading to formation of the complex **I′**. Path C starts with deprotonation of the methyl ligand, followed by H* migration from the Os center to the methylene group, and finally leads to **I′** by protonation of Os. The reverse of this path, deprotonation from the Os−H bond followed by H* migration and protonation, is also possible. The first step of paths D and E is the reductive elimination (formation of a C−H* bond) leading to the methane complex [Os](CH_3H^*), **VI**. From this complex the reaction splits into the two different paths. Path D, called the H-exchange path, proceeds via the methane rearrangement and methane oxidative addition (C−H bond activation) transition state and leads to the final complex **I′**. Path E, called the "dissociation/association" mechanism, also starts from complex **VI** and proceeds via dissociation of the CH_3H^* molecule, followed by its re-coordination and C−H bond activation leading to complex **I′**.

During the preparation of the manuscript, a DFT study of the mechanism of this hydrogen scrambling reaction for a model system was published by Martin.[2] Our conclusions are basically similar to those of Martin,[2] but here we provide more detailed studies on all of the postulated mechanisms, compare the free energy as well as the energy, study the substitution effects on the reaction energetics by calculating the real (experimen-

(1) Gross, C. L.; Girolamin, G. S. *J. Am. Chem. Soc.* **1998**, *120*, 6605.

(2) Martin, L. *J. Am. Chem. Soc.* **1999**, *121*, 9459.

10.1021/om010776o CCC: $22.00
Publication on Web 12/21/2001

Scheme 1

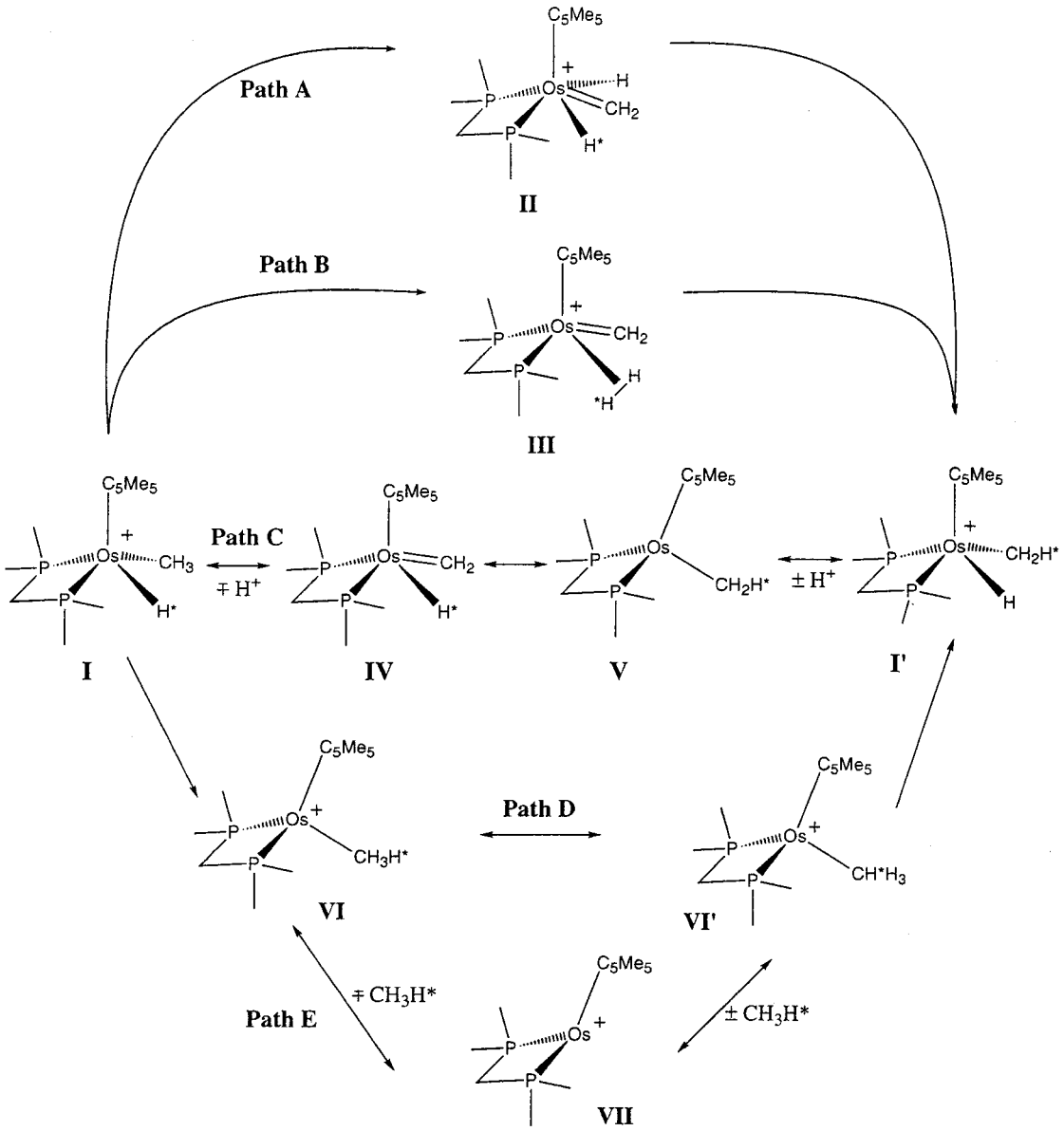

tally used) complex, and elucidate the role of solvent effects.

This paper is organized as follows. In section II, the calculation procedure is described. In section III, we discuss our results. In section III.A, all possible isomers of the model complex $[CpOs(PH_2CH_2PH_2)(CH_3)H^*]^+$, **1**, will be discussed. In section III.B, we discuss all proposed pathways and the intermediate located on these pathways, while in section III.C we study in more detail the pathways D and E. Section III.D is devoted to the discussions of the role of solvent effects in the H-scrambling in the model complex **1**. In section III.E the H-scrambling pathways D and E in the experimentally used real complex $[Cp^*Os(PMe_2CH_2PMe_2)(CH_3)H^*]^+$, **I**, including all nine methyl substituents, will be discussed. In section IV, we draw conclusions from these studies.

II. Calculation Procedure

At the first stage of our studies we used the complex $[CpOs(PH_2CH_2PH_2)(CH_3)H^*]^+$, **1** (where $Cp = C_5H_5$), as a model of **I**. Later, we extend our studies to the experimentally used complex **I** by including all nine methyl groups in the calculations. Below, we will denote all intermediates and transition states of model studies by an Arabic numbers, while Roman numbers will be used for real systems. The geometries of model complexes were optimized using the B3LYP hybrid density functional theory[3−5] with a standard double-ζ quality basis set (Lanl2dz) associated with the relativistic effective core potential for osmium[6] and phosphorus,[7] and the valence double-ζ basis set for other atoms.[8] Previously, the B3LYP method with a double-ζ quality basis set has been shown to be quite reliable both in geometry and energy.[9]

The potential energy surface of the reaction of the real system, **I**, was studied with the integrated MO + MO method, ONIOM (also called IMOMO).[10] In the ONIOM method, a "low" level calculation is performed for the "real" system and both "high" and "low" level calculations are carried out for a smaller

(3) Becke, A. D. *Phys. Rev. A* **1998**, *38*, 3098.
(4) Lee, C.; Yang, W.; Parr, R. G. *Phys. Rev. B* **1988**, *37*, 785.
(5) Becke, A. D. *J. Chem. Phys.* **1993**, *98*, 5648.
(6) Wadt, W.R.; Hay, P. J. *J. Chem. Phys.* **1985**, *82*, 284.
(7) Hay, P. J.; Wadt, W. R. *J. Chem. Phys.* **1985**, *82*, 270.
(8) Dunning, T. H., Jr.; Hay, P. J. In *Modern Theoretical Chemistry*; Schaefer, H. F., III, Ed.; Plenum: New York, 1976; Vol. 3, p 1.

"model" system, which was cut out from the "real" system. The ONIOM energy of the "real" system is defined as

$$E(\text{ONIOM, real}) = E(\text{high, model}) + E(\text{low, real}) - E(\text{low, model})$$

as an approximation for the "high" level calculation for the "real" system. In the present case, the "real" system is complex **I**, while the "model" system is complex **1**. The "high" level is B3LYP/Lanl2dz, the same as above, while the "low" level is the Hartree−Fock (HF) method with a minimum basis set, Lanl2mb. Thus, the ONIOM method used in this paper can be denoted as ONIOM (B3LYP/Lanl2dz:HF/Lanl2mb).

Since the experiments[1] were carried out in a polar solvent ($CDFCl_2$), we also studied the role of solvent on the mechanism of H-scrambling in the model complex **1**. In these calculations we have used a polarizable continuum method (PCM)[11] with a dielectric constant of 4.9 (the experimental value for $CHCl_3$).

The nature of all the calculated equilibrium structures and transition states was confirmed by performing normal coordinate analyses. Zero-point-corrected energies (ΔE + ZPE) and Gibbs free energies (ΔG at 1 atm and 278.15 K) were calculated for each stationary point. All calculations were performed with the Gaussian98 package.[12]

III. Results and Discussions

A. Structural Isomers of Model Complex 1. At first, let us discuss the possible isomers of the complex **1**. In general, it may have four different isomers defined by cis/trans positioning of the hydride and alkyl ligands and bidentate/monodentate coordination of the bisphosphine ligand. However, our calculations found only three stable isomers, **1a** (cis), **1b** (trans), and **1c** (monodentate), shown in Figure 1. In this figure, we also present the cis **1a** ↔ trans **1b** isomerization transition state **1d**. Since only the cis isomer was detected experimentally,[1] below we consider **1a** as a reference for the relative energy calculation.

The calculations show that the cis isomer, **1a**, is energetically by (1.6)[1.4] kcal/mol less favorable than trans isomer **1b**. (Here and below we will present the zero-point-corrected energies with parentheses, while Gibbs free energies will be given in brackets.) As seen in Figure 1, the calculated geometry of the cis isomer **1a** has a distorted square pyramidal symmetry with the Cp ligand in the apical position. The calculated Os−P distances are different by 0.016 Å, which is consistent with the available NMR data indicating the nonequivalency of the two phosphorus atoms in complex **I**. Meantime, the trans isomer **1b** looks more like bipyramidal with hydride and alkyl groups in the axial position. The Cp carbons are 2.27−2.43 Å and 2.26−2.37 Å away from the Os in **1a** and **1b**, respectively. The Os−H* and Os−CH_3 bonds in **1b** are slightly longer than in **1a** due to the strong trans influence of alkyl and hydride ligands, respectively. In **1b**, the H*−Os−CH_3 angle is as large as 141°, which obviously prevents a direct hydrogen exchange in this complex.

These two isomers, **1a** and **1b**, are separated by the transition state, **1d**, which has one imaginary frequency of 66i cm^{-1}. The IRC calculations confirmed that **1d** connects isomers **1a** and **1b**. A comparison of the geometries of **1d** with those of **1a** and **1b** indicates that **1d** is an early transition state; the geometry of **1d** is very close to that of **1a**. The cis−trans isomerization barrier is calculated to be (9.9)[10.5] kcal/mol, relative to the isomer **1a**. This barrier is large enough to prevent cis−trans isomerization at low temperature. Since the trans isomer was not observed by experimentalists in the given conditions, the barrier for cis ↔ trans isomerization has to be higher than that for hydrogen scrambling. Therefore, intermediates and transition states that lie higher than the transition state **1d** could be eliminated from the discussions.

The third, monodentate bisphosphine isomer **1c**, with a quasi-tetrahedral Os center, lies (15.2)[13.8] kcal/mol higher in energy than **1a** and is expected not to play any role in the hydrogen exchange reaction. Although we have not studied the cis ↔ trans isomerization for isomer **1c**, one expects it to occur more easily for monodentate bisphosphine isomer **1c** than for its bidentate analogue **1a**.

B. Intermediates for H-Exchange between Hydride and Methyl Ligands. As discussed above, starting from **1a** (which is the model of **I**), the hydrogen scrambling may occur via at least five different pathways summarized in Scheme 1. The equilibrium structures of intermediates **2**−**5** (which are models of the real complexes **II**−**V**, respectively, given in Scheme 1) located on these pathways are presented in Figure 2.

Path A. First, let us discuss the intermediate **2** located on path **A**, the oxidative addition pathway. Intermediate **2**, the product of oxidative addition of the methyl C−H bond, exists only as a monodentate bisphosphine complex, as seen in Figure 2. In other words, the Os center of **1a** has to de-coordinate one of the phosphine legs in order to accommodate the coming

(9) (a) Musaev, D. G.; Morokuma, K. *J. Phys. Chem.* **1996**, *100*, 6509. (b) Erikson, L. A.; Pettersson, L. G. M.; Siegbahn, P. E. M.; Wahlgren, U. *J. Chem. Phys.* **1995**, *102*, 872. (c) Ricca, A.; Bauschlicher, C. W., Jr. *J. Phys. Chem.* **1994**, *98*, 12899. (d) Heinemann, C.; Hertwig, R. H.; Wesendrup, R.; Koch, W.; Schwarz, H. *J. Am. Chem. Soc.* **1995**, *117*, 495. (e) Hertwig, R. H.; Hrusak, J.; Schroder, D.; Koch, W.; Schwarz, H. *Chem. Phys. Lett.* **1995**, *236*, 194. (f) Schroder, D.; Hrusak, J.; Hertwig, R. H.; Koch, W.; Schwerdtfeger, P.; Schwarz, H. *Organometallics* **1995**, *14*, 312. (g) Fiedler, A.; Schroder, D.; Shaik, S.; Schwarz, H. *J. Am. Chem. Soc.* **1994**, *116*, 10734. (h) Fan, L.; Ziegler, T. *J. Chem. Phys.* **1991**, *95*, 7401. (i) Berces, A.; Ziegler, T.; Fan, L. *J. Phys. Chem.* **1994**, *98*, 1584. (j) Lyne, P. D.; Mingos, D. M. P.; Ziegler, T.; Downs, A. J. *Inorg. Chem.* **1993**, *32*, 4785. (k) Li, J.; Schreckenbach, G.; Ziegler, T. *J. Am. Chem. Soc.* **1995**, *117*, 486.

(10) (a) Humbel, S.; Sieber, S.; Morokuma, K. *J. Chem. Phys.* **1996**, *105*, 1959. (b) M. Svensson, Humbel, S.; Froese, R. D. J.; Matsubara, T.; Sieber, S.; Morokuma, K. *J. Phys. Chem.* **1996**, *100*, 19357. (c) Dapprich, S.; Komaromi, I.; Byun, K. S.; Morokuma, K.; Frisch, M. J. *J. Mol. Struct. (THEOCHEM)* **1999**, *461*−*462*, 1. (d) Vreven, T.; Morokuma, K. *J. Comput. Chem.* **2000**, *21*, 1419.

(11) Cossi, M.; Barone, V.; Cammi, R.; Tomasi, J. *Chem. Phys. Lett.* **1996**, *255*, 327. Also see: (a) Miertus, S.; Scrocco, E.; Tomasi, J. *Chem. Phys.* **1981**, *55*, 117. (b) Pascual-Ahuir, J. L.; Silla, E.; Tomasi, J.; Bonaccorsi, R. *J. Comput. Chem.* **1987**, *8*, 778. (c) Floris, F.; Tomasi, J. *J. Comput. Chem.* **1989**, *10*, 616. (d) Tomasi, J.; Persico, M. *Chem. Rev.* **1994**, *94*, 2027. (e) Cossi, M.; Barone, V.; Cammi, R.; Tomasi, J. *J. Chem. Phys.* **1997**, *107*, 3032. (f) Barone, V.; Cossi, M.; Tomasi, J. *J. Comput. Chem.* **1998**, *19*, 404.

(12) Frisch, M. J.; Trucks, G. W.; Schlegel, H. B.; Scuseria, G. E.; Robb, M. A.; Cheeseman, J. R.; Zakrzewski, V. G.; Montgomery, J. A., Jr.; Stratmann, R. E.; Burant, J. C.; Dapprich, S.; Millam, J. M.; Daniels, A. D.; Kudin, K. N.; Strain, M. C.; Farkas, O.; Tomasi, J.; Barone, V.; Cossi, M.; Cammi, R.; Mennucci, B.; Pomelli, C.; Adamo, C.; Clifford, S.; Ochterski, J.; Petersson, G. A.; Ayala, P. Y.; Cui, Q.; Morokuma, K.; Malick, D. K.; Rabuck, A. D.; Raghavachari, K.; Foresman, J. B.; Cioslowski, J.; Ortiz, J. V.; Baboul, A. G.; Stefanov, B. B.; Liu, G.; Liashenko, A.; Piskorz, P.; Komaromi, I.; Gomperts, R.; Martin, R. L.; Fox, D. J.; Keith, T.; Al-Laham, M. A.; Peng, C. Y.; Nanayakkara, A.; Gonzalez, C.; Challacombe, M.; Gill, P. M. W.; Johnson, B.; Chen, W.; Wong, M. W.; Andres, J. L.; Gonzalez, C.; Head-Gordon, M.; Replogle, E. S.; Pople, J. A. *Gaussian 98*, revision A.7; Gaussian, Inc.: Pittsburgh, PA, 1998; p 8.

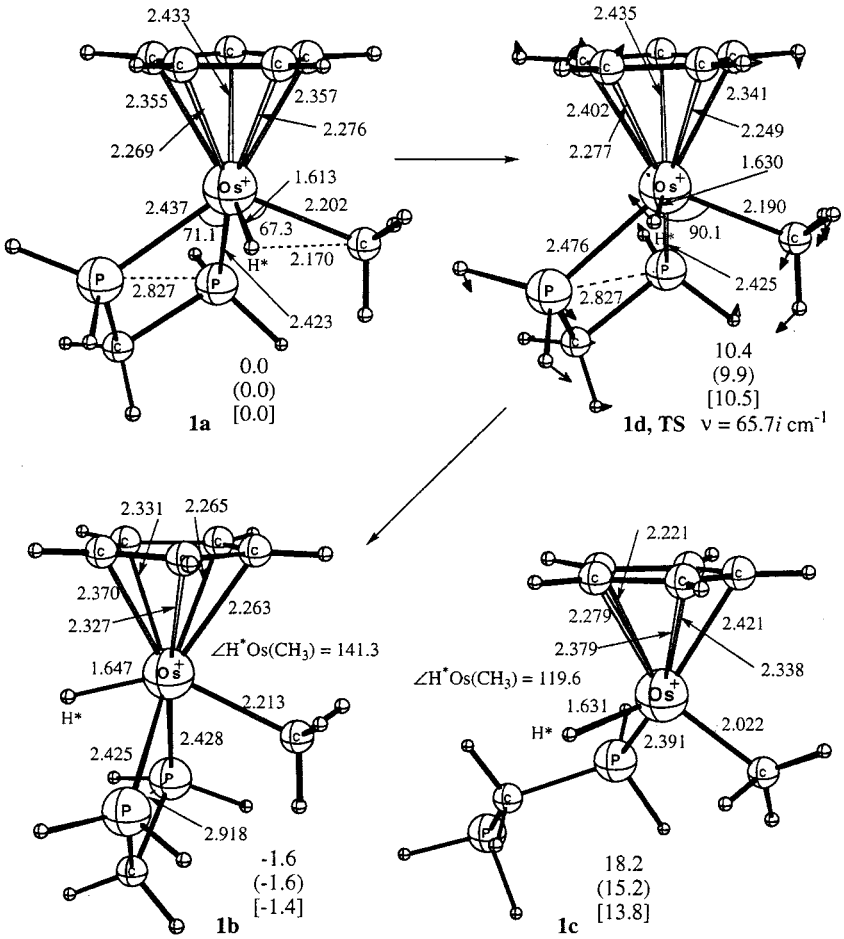

Figure 1. Optimized structures (distances in Å and angles in deg) and relative energies (ΔE without parentheses, ΔE + ZPC with parentheses, and ΔG in brackets, in kcal/mol) of the stable isomers of complex **1**—**1a** (cis), **1b** (trans), and **1c** (monodentate)—and transition state connecting **1a** and **1b**. For the transition state, the reaction coordinate (denoted by the arrows) and its imaginary frequency are shown.

hydride ligand. The complex remains square pyramidal, with trans hydrides (H−Os−H* angle: 131.4°) and trans-positioned terminal phosphine and carbene (H_2C−Os−P angle: 103.2°) ligands in the basal positions. The apical position is occupied by the η^5-coordinated Cp ring. The intermediate **2** is calculated to be (20.8)[18.9] kcal/mol higher in energy than reactant **1a**.

Path B. Now we will discuss the intermediate **3** on path B, the σ-bond metathesis pathway. The optimization of the geometries of **3** with a dihydrogen ligand converged to the cis-dihydride complex with an alkyl phosphonium ligand, presented in Figure 2, with Os−H, H−H, and Os−CH_2(P) distances of 1.61−1.63, 1.705, and 2.168 Å, respectively. Complex **3** is energetically more stable than **2** by (9.9)[7.6] kcal/mol and lies (10.9)-[11.3] kcal/mol higher than **1a**.

Path C. Pathway C proceeding via the deprotonation of **1a** to form intermediates **4** and then **5** is energetically very (about 240 kcal/mol if H^+ dissociates as proton, and about 70 kcal/mol if H^+ leaves to form H_3O^+) unfavorable. As seen in Figure 2, to form the Os−C double bond in complex **4**, one of the phosphine legs has to dissociate. In the alkyl complex **5**, which has C_s-symmetry, the phosphine ligand is bidentately coordinated, where the Os−P distances are shorter than in **1a**.

Paths D and E. The common intermediate of pathways D and E is complex **6**. In complex **6**, an ion-molecular complex $[(C_5H_5)Os(PH_2CH_2PH_2)]^+\cdots(CH_3H^*)$, the methane molecule is coordinated to the Os atom asymmetrically, somewhere between η^1 and η^2 coordination mode (most likely with one side-on coordinated C−H bond), as shown in Figure 3, with a short (1.948 Å) Os−H* and a long (2.800 Å) Os−H bond. The nonequivalency of the two ends of the bisphosphine ligand still exists. Complex **6** is nearly isoenergetic to complex **1a**.

Complex **7**, which is complex **6** without the methane molecule and is on path E, has a C_s-symmetrical structure. The binding energy of methane, the energy difference between dissociation limit **7** + CH_4 and **6**, is calculated to be 7.3 kcal/mol in ΔE + ZPC and −3.6 kcal/mol in ΔG, indicating that the free energy favors methane dissociation.

A comparison of the calculated energetics of the expected intermediates of pathways A−E with each other, as well as with the energy barrier corresponding to cis **1a** ↔ trans **1b** isomerization, shows that complexes **2**, **3**, and **4** and **5**, intermediates of pathways A, B, and C, respectively, lie significantly higher in energy than those for paths D and E, as well as the **1a** ↔ **1b** isomerization barrier. Therefore, these pathways can be eliminated from further discussions. Only complexes **6** and **7**, intermediates of paths D and E, are the lowest in energy and lie lower than the **1a** ↔ **1b** isomerization barrier. Therefore, the main mechanism of the hydrogen scrambling process in **1a** is likely to be path D or E,

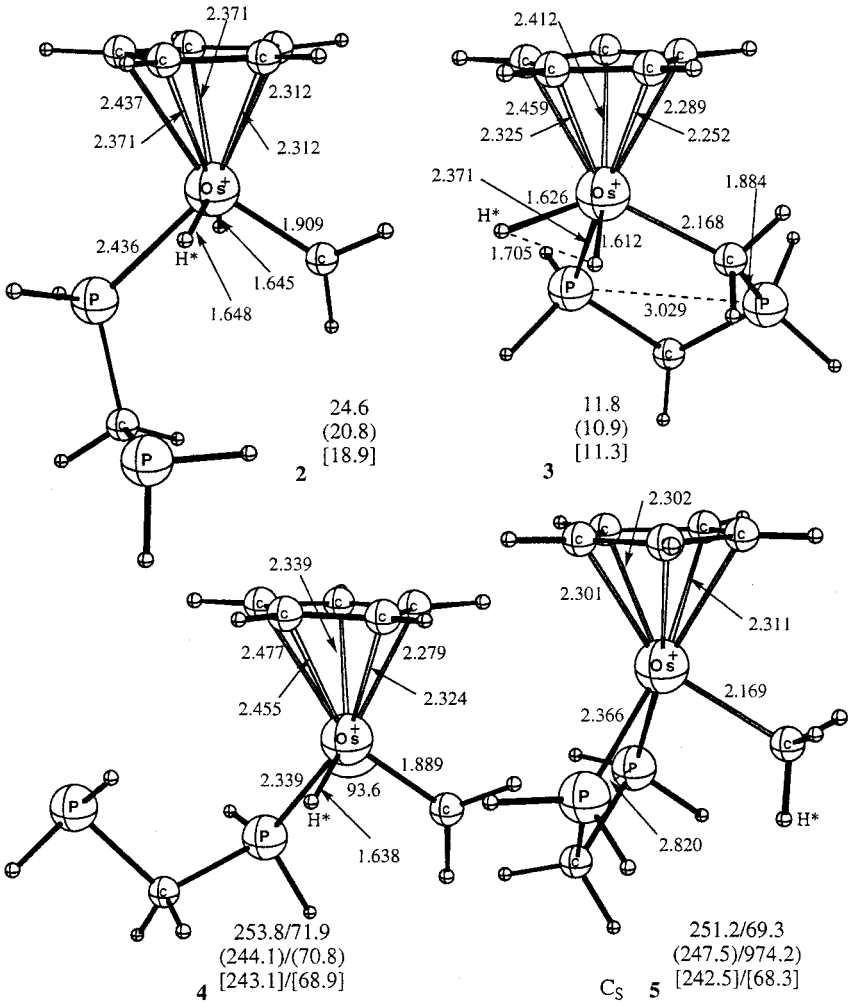

Figure 2. Optimized structures (distances in Å and angles in deg) and relative energies (ΔE without parentheses, ΔE + ZPC with parentheses, and ΔG in brackets, in kcal/mol relative to **1a**) of the intermediates **2**−**5**. For intermediates **4** and **5**, energies before the slash are for the reaction **1a** → **4** (or **5**) + H^+, while after slash for the reaction **1a** + H_2O → **4** (or **5**) + OH_3^+.

which will be discussed in more detail in the next section.

C. Potential Energy Surface of Hydrogen Exchange Pathways D and E for the Model System. The first steps of the paths D and E are the same and correspond to the reductive elimination from **1a** to form the methane complex $[(C_5H_5)Os(PH_2CH_2PH_2)]^+(CH_3H^*)$, **6**. The transition state (TS) **8** is presented in Figure 3. Normal-mode analysis confirms that this is the real TS with one imaginary frequency, 769.5i cm^{-1}, corresponding to C−H* bond formation. The IRC calculations following this reaction coordinate confirmed that TS **8** connects **1a** and **6**. As seen in Figures 1 and 3, upon going from **1a** to TS **8**, the C−H* distance decreases from 2.170 to 1.494 Å. Meantime, the breaking Os−H* and Os−C bonds elongate from 1.613 and 2.202 Å to 1.657 and 2.338 Å, respectively. Other geometry parameters did not change significantly. These geometry changes are consistent with the nature of TS **8**. The energy barrier for this process is calculated to be (6.0)[6.0] kcal/mol, which is significantly smaller than the **1a** ↔ **1b** isomerization barrier, (9.9)[10.5] kcal/mol, at **1d**, reported above. After overcoming the TS **8**, the reaction leads to complex **6**, where the methane molecule CH_3H^* is coordinated to the Os center asymmetrically with its H*−C bond.

From complex **6** the reaction may proceed via two different pathways, D and E. Pathway D is symmetric and involves an equivalent methane complex, called **6′**, with a long Os−H* and a short Os−H bond, separated from complex **6** by the "methane rearrangement" transition state **9** in C_s symmetry, shown in Figure 3. Normal-mode analysis confirms that this is a real TS with one imaginary frequency, 321.5i cm^{-1}. The IRC calculations confirmed that TS **9** connects **6′** with **6**. In TS **9**, the methane molecule is coordinated to Os in a bidentate manner with H* and one of the H atoms. The equivalent Os−H distances are 2.334 Å, and the Os−C distance is 2.737 Å. The energy barrier corresponding to this process is calculated to be (1.6)[1.6] kcal/mol. In the next step, the resultant complex **6′** undergoes C−H oxidative addition via exactly the same transition state as **8**, TS **8′**, and leads to the hydridomethyl complex **1a′**, (H)[Os](CH2H*). The energy barrier for this process at TS **8′** is (6.2)[7.1] kcal/mol.

Another process starting from complex **6** corresponds to pathway E, the "dissociation/association" mechanism. It proceeds via dissociation of the CH_3H^* molecule from **6** to form coordinatively unsaturated complex **7**, followed by re-coordination of CH_3H^* to **7** via its C−H bond, and leads to complex **1a′**. The methane dissociation from **6** is calculated to be 7.3 kcal/mol endothermic using ΔE

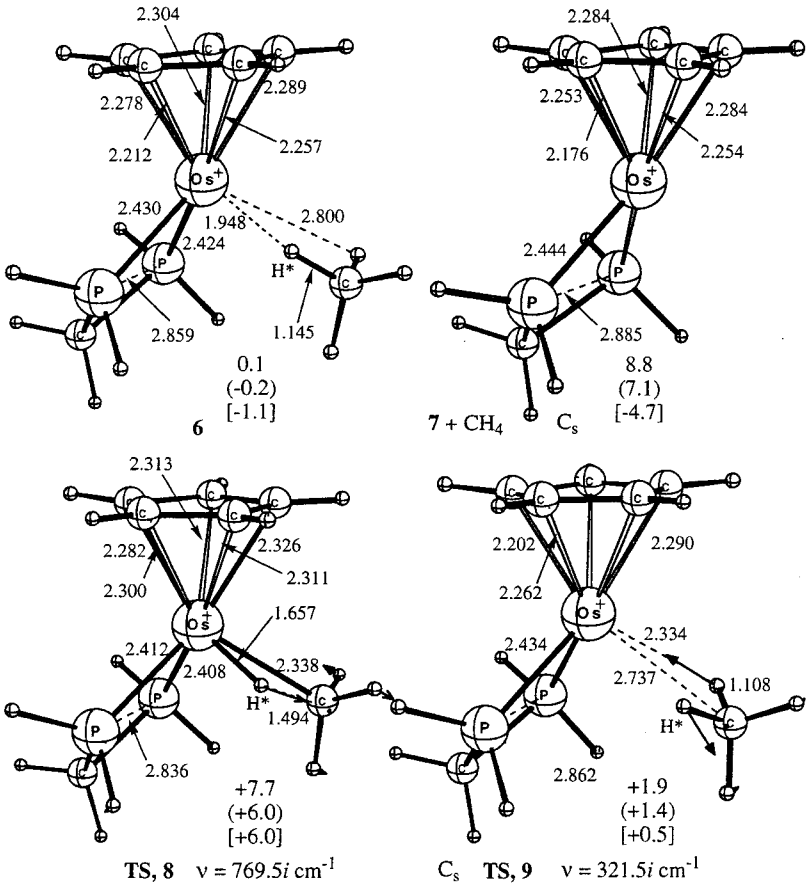

Figure 3. Optimized structures (distances in Å and angles in deg) and relative energies (ΔE without parentheses, ΔE + ZPC with parentheses, and ΔG in brackets, in kcal/mol relative to **1a**) of the intermediates (**6** and **7**) and transition states (**8** and **9**) of paths D and E. For the transition state, the reaction coordinate (denoted by the arrows) and its imaginary frequency are shown.

+ ZPC and 3.6 kcal/mol exothermic in ΔG; at the normal temperature, the entropy favors the methane dissociation pathway.

Note that the methane dissociation was considered a barrierless process in the previous studies.[1,2] However, the calculated ΔG value of intermediate **7** + CH_4, which is 3.6 kcal/mol lower than complex **6**, suggests the possible existence of an entropy-related barrier. By performing potential energy surface scanning using the Os−C distance as a reaction coordinate, we were able to locate this transition state. The ΔE + ZPE energy increases monotonically from **6** to **7** + CH_4, and there exists no transition state. The Gibbs free energy barrier was found at the Os−C bond of ∼4.5 Å, 2.4 kcal/mol above complex **6**.

In Figure 4, we have summarized the energy profiles of the H-scrambling in **1a**, which could occur via either path D or E. As seen from this figure, the ΔE + ZPE energetics indicates that the process proceeds via an H-exchange mechanism (path D) with a 6.2 kcal/mol rate-determining barrier from **6′** to TS **8′**. The dissociative/associative mechanism corresponding to path E and proceeding via dissociation of the methane molecule is unfavorable, because it requires 7.3 kcal/mol for methane dissociation, instead of 1.6 kcal/mol for methane rearrangement at TS **9**. The same conclusion on the basis of the ΔE + ZPE energetics has been made previously by Martin.[2] However, taking entropy effects into consideration, ΔG changes this conclusion. As seen in Figure 4, entropy effects only slightly change the energetics of the transition states and intermediates located on the H-exchange pathway (path D), while they significantly (11.8 kcal/mol) stabilize the methane dissociation limit **7** + CH_4 on path E. As a result and because of the existence of the entropy-related methane elimination barrier of 2.4 kcal/mol, the dissociative/associative mechanism (path E) becomes comparable in energy with the H-exchange pathway (path D) and may compete in the real system.

The calculated rate-determining barrier heights for H-scrambling in **1a** of $(\Delta E + \text{ZPE})^{\ddagger} = (6.0)$ and $\Delta G^{\ddagger} = 8.1$ kcal/mol at 278.15 K, 1 atm, at TS **8** agree reasonably well with the experimentally reported values in **I**, $\Delta H^{\ddagger} = 7.1 \pm 0.9$ kcal/mol and $\Delta G^{\ddagger} = 8.1$ kcal/mol at −100 °C, 1 atm, and Martin's[2] calculated $(\Delta E + \text{ZPE})^{\ddagger}$ value of 9.2 kcal/mol. Meantime, the experiment reported the activation free energy for reductive elimination to be $\Delta G^{\ddagger} = 13.5$ kcal/mol at −100 °C, attributed to a different transition state. Our finding is that the transition state **8** is common for both H-exchange and dissociative/associative mechanisms. The final dissociation of methane from the product complex **6** is endothermic by 7.3 kcal/mol in ΔE + ZPE and occurs without energetic barrier; the entropy effects at 278.15 K and 1 atm make methane dissociation from complex **6** exothermic by 3.6 kcal/mol, while it introduces a 2.4 kcal/mol reductive elimination barrier calculated from **6**. Note that the methane dissociation from the product complex **6** is nearly thermoneutral (+0.3 kcal/mol) at −100 °C and 1 atm (experimentally reported conditions).

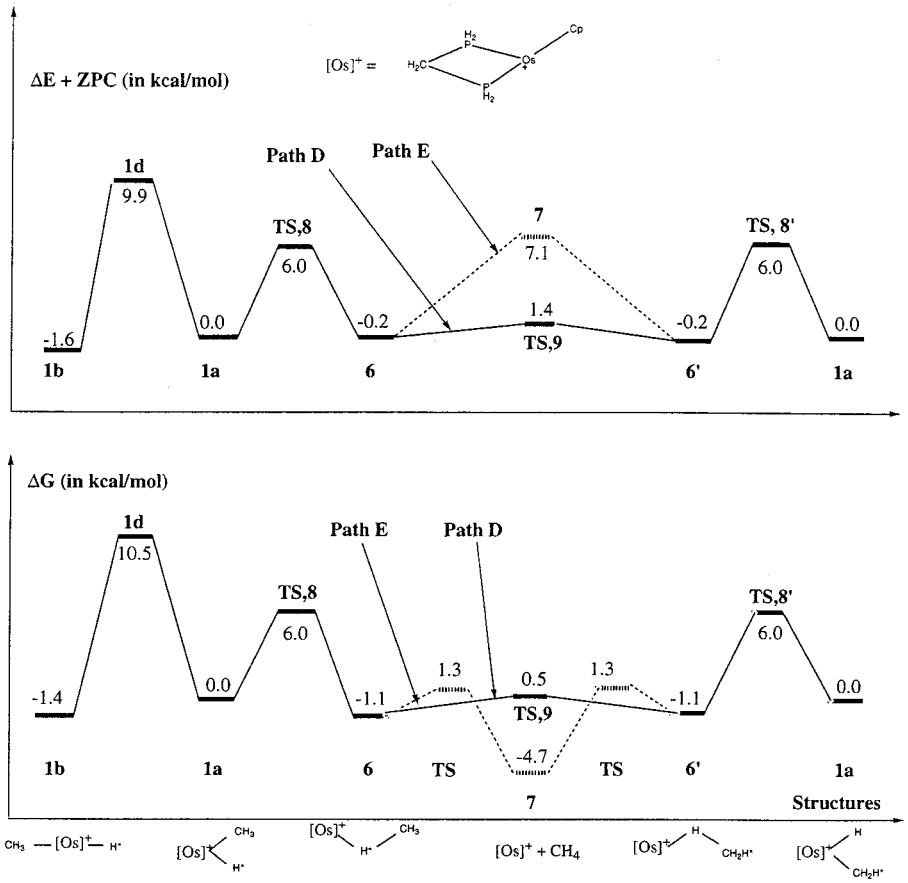

Figure 4. Energy profiles (ΔE + ZPC and ΔG) of H-scrambling in the model complex **1a** for paths D and E.

Table 1. Comparison of the Calculated Relative Energies, ΔE + ZPC and ΔG, in the Gas Phase with Those, $\Delta E_{Solution} = \Delta G_{sol}$ + ZPC and $\Delta G_{solution} = \Delta G_{sol} + (\Delta G_{gas} - \Delta E_{gas})$, in $CHCl_3$ Solution for the Model System $[(C_5H_5)Os(PH_2CH_2PH_2)(CH_3)H]^+$

	PCM (single point)		PCM (reoptimized)		gas phase	
structure	$\Delta E_{solution}$	$\Delta G_{solution}$	$\Delta E_{solution}$	$\Delta G_{solution}$	ΔE + ZPC	ΔG
1a	0.0	0.0	0.0	0.0	0.0	0.0
TS, **1d**	10.0	10.1			9.9	10.5
1b	−1.2	−1.0	−1.1	-0.9	−1.6	−1.4
TS, **8**	8.9	8.9	9.0	9.0	6.0	6.0
6	2.6	1.4	2.6	1.4	−0.2	−1.1
TS, **9**	4.1	2.7	4.3	2.9	1.4	0.5
7 + CH_4	9.7	−3.8	9.6	−3.9	7.1	−4.7

We could not find any process corresponding to $\Delta G^{\ddagger} = 13.5$ kcal/mol. Although we tend to agree with Martin[2] that this experimental value may simply be a measure of the stability of an intermediate, there also is a possibility that this discrepancy can be a result of (a) the solvent effects and (b) the electronic and steric effects from the methyl ligands of Cp* and $(Me)_2PCH_2P(Me)_2$ groups, neither of which was included in the above calculations. The following studies on the role of solvent effects and the electronic and steric effects from the methyl ligands of Cp* and $(Me)_2PCH_2P(Me)_2$ groups should provide some additional answers to the problem.

D. Solvent Effects for the Model System. The energies in solution of the important intermediates and transition states calculated with the PCM method are summarized in Table 1. Here, we have performed two types of calculation: the single-point PCM calculation using the optimized geometries in gas phase and geometry re-optimization of intermediates and transition states in the presence of the solvent PCM. In these calculations we used $\epsilon = 4.9$, the experimental value for $CHCl_3$. At first, PCM optimization of the geometries shows that the geometry changes in the presence of solvent are insignificant, and therefore, these changes will not be discussed here. Second, as seen in Table 1, reoptimization of the geometries at the PCM level has a very small (0.2 kcal/mol) effect on the energies. These results are consistent with the previous studies; several groups have shown that, unless the system is ionic or very polar, reoptimization of the geometries has very limited effect on the computed solvation energies.[13−17]

The PCM ΔG_{sol} includes the energy of the solute in solution with all the energetic and entropic effects of the solvent in a semiempirical manner. Since we were

(13) Barone, V.; Cossi, M.; Tomasi, J. *J. Chem. Phys.* **1997**, *107*, 3210.
(14) Pomeli, C. S.; Tomasi, J.; Sola, M. *Organometallics* **1998**, *17*, 3164.
(15) Cacelli, I.; Ferretti, A. *J. Chem. Phys.* **1998**, *109*, 8583.
(16) Creve, S.; Oevering, H.; Coussens, B. B. *Organometallics* **1999**, *18*, 1907.
(17) Bernardi, F.; Bottoni, A.; Miscone, G. P. *Organometallics* **1998**, *17*, 16.

unable to calculate the vibrational frequencies of the solute transition states and intermediates with the PCM, below we use the gas-phase values calculated in the preceding sections for the solute zero-point energy and entropy corrections and add them to ΔG_{sol}. We believe that this approach is acceptable for the given case, since there are only slight differences between the gas-phase and solution structures. Thus, below we will report and discuss only $\Delta E_{solution} = \Delta G_{sol} + ZPC_{gas}$ and $\Delta G_{solution} = \Delta G_{sol} + (\Delta G_{gas} - \Delta E_{gas})$ values, which could be compared with ΔE + ZPC and ΔG values from the gas-phase studies.

The comparison of the relative energies (with respect to **1a**) calculated in the gas phase and in solution, given in the Table 1, shows that the effects of solvation on the energies of the complex **1b** as well as transition state **1d** are small; solvent effects decrease cis−trans isomerization energy by (0.4)[0.4] kcal/mol and increase the barrier between **1a** and **1b** (calculated from **1b**) by (0.3)-[0.8] kcal/mol. However, solvent effects significantly destabilize the transition states **8** for C−H* bond formation and **9** for "methane rearrangement" as well as the methane complex **6** and the dissociation limit **7** + CH_4. As a result, the barrier height separating complex **1a** from **6** at transition state **8** on paths D and E is changed from (6.0)[6.0] kcal/mol in the gas phase to (8.9)[8.9] kcal/mol in solution, while the barrier separating complex **6** from **6′** at transition state **9** on path D changed only slightly from (1.6)[1.6] in the gas phase to (1.5)[1.3] kcal/mol in solution. Similar effects were observed for the methane dissociation from the complex **6** → **7** + CH_4; in the gas phase, this process was calculated to be endothermic (+7.3 kcal/mol) in ΔE + ZPE but exothermic [−3.6 kcal/mol] in ΔG values. In solution phase it becomes endothermic by (+7.1) kcal/mol in $\Delta E_{solution}$ level, while exothermic [−5.2] kcal/mol in $\Delta G_{solution}$.

Thus, in $CHCl_3$ solution the reaction mechanism has not changed from the gas phase. In $CHCl_3$ solution the rate-determining barrier for hydrogen scrambling in **1a** remains the process of C−H* bond formation occurring via (8.9)[8.9] kcal/mol barrier at transition state **8** and leading to the formation of complex **6**. From complex **6**, the process most likely will proceed via the H-exchange mechanism (path D in Scheme 1): **6** → TS **9** → **6′** → TS **8′** → **1b′**, with the largest barrier of (6.3)[7.5] kcal/mol at TS **8′** for C−H bond activation. However, again, inclusion of entropy factors ($\Delta G_{solution}$) makes path E via methane dissociation competitive, and this may actually take place.

E. Potential Energy Surface of the Real System for Pathways D and E. In the above studies, we used Cp and $PH_3CH_2PH_3$ as model ligands. In the real system, Cp* and dmpm ligands are used. To elucidate the role of the electronic and steric effects of the nine methyl ligands on the H-scrambling process and methane elimination, we studied the real system **I** with the ONIOM method and compared the results with the model system **1** reported above. The structure and relative energies of intermediates and transition states of the real system **I** are summarized in Figure 5. Comparison of the calculated equilibrium geometries of real complexes **Ia** and **Ib** with those of corresponding model complexes **1a** and **1b** (Figure 1) shows only small differences in the bond lengths and bond angles. The Os−P, Os−H*, and Os−CH_3 distances are quite similar, and there is no systematic change in the position and coordination of the Cp* ring. However, significant differences between the model (see Figure 3) and real complexes were found for the methane complexes, **6** and **VI**, and for the transition states **8**, **9** and **VIII**, **IX**, respectively. In all of these cases, the methane moiety of the "real" complexes tends to be further away from the Os center by 0.04−0.08 Å, and consequently, the C−H* bond distance is shorter in "real" systems than in model ones. These results can be explained in terms of both steric and electronic effects of the methyl substituents in Cp* and dmpm ligands in the "real" systems.

Despite the relatively small structural effects from the bulkier and more electron-donating substituents in the "real" system, there are notable energetic changes in the H-scrambling potential profile of the "real" system, as shown in Figure 6, compared to that for the "model" system (see Figure 4). The energy difference between the more stable trans and the cis isomer is larger, (2.9)-[3.0] kcal/mol in the "real" system vs (1.6)[1.4] kcal/mol in the "model" system. For the "real" system, the barrier for reductive elimination (C−H* bond formation) at the transition state **VIII**, (8.8)[8.5] kcal/mol, is 2.5−2.8 kcal/mol higher than that for the model system (**8**), (6.0)-[6.0] kcal/mol. In the "real" system, the process **Ia** → **VI** is found to be endothermic by (5.9)[4.5] kcal/mol, while in the "model" system it was slightly, (0.2)[1.1] kcal/mol, exothermic. In other words, methyl substituents destabilize, relative to **Ia**, the methane complex **VI** and transition states nearby by a few to several kcal/mol. As a result, the methane oxidative addition barrier at **VIII′** from **VI′** is reduced significantly to (2.9)[4.0] kcal/mol for the "real" system from (6.2)[7.1] kcal/mol for the "model" system. Destabilization of the methane complex **VI′**, relative to the TS **VIII′**, in the "real" system significantly reduces the methane C−H bond activation barrier.

The methane rearrangement transition state, TS **IX**, is destabilized to an extent similar to the methane complex **VI** upon going from the "model" system to the "real" one. As a result, the methane rearrangement barrier from the methane complex **VI** is only slightly reduced from (1.6)[1.6] kcal/mol for the model system to (1.0)[0.5] kcal/mol for the "real" system. As expected, the methane dissociation energy also is reduced in the "real" system: (3.6)[−7.2] kcal/mol in the "real" system vs (7.3)[−3.6] kcal/mol in the "model" system. As discussed for the structural changes, these trends are due to both steric and electronic effects of the methyl substituents in Cp* and dmpm ligands in the "real" systems. Note that for "real" system we have not studied the TS separating complex **VI** and the dissociation limit **VII** + CH_4. However, we still believe the existence of an entropy-related barrier of a few kcal/mol for the process **VI** ↔ **VII** + CH_4.

Thus, the nine methyl substituents on the ligands did not change our main conclusions obtained from the "model" studies. They destabilized the methane complex and nearby transition states by a few to several kcal/mol. In the real system, as in the model system, the rate-determining step is the C−H* bond formation process

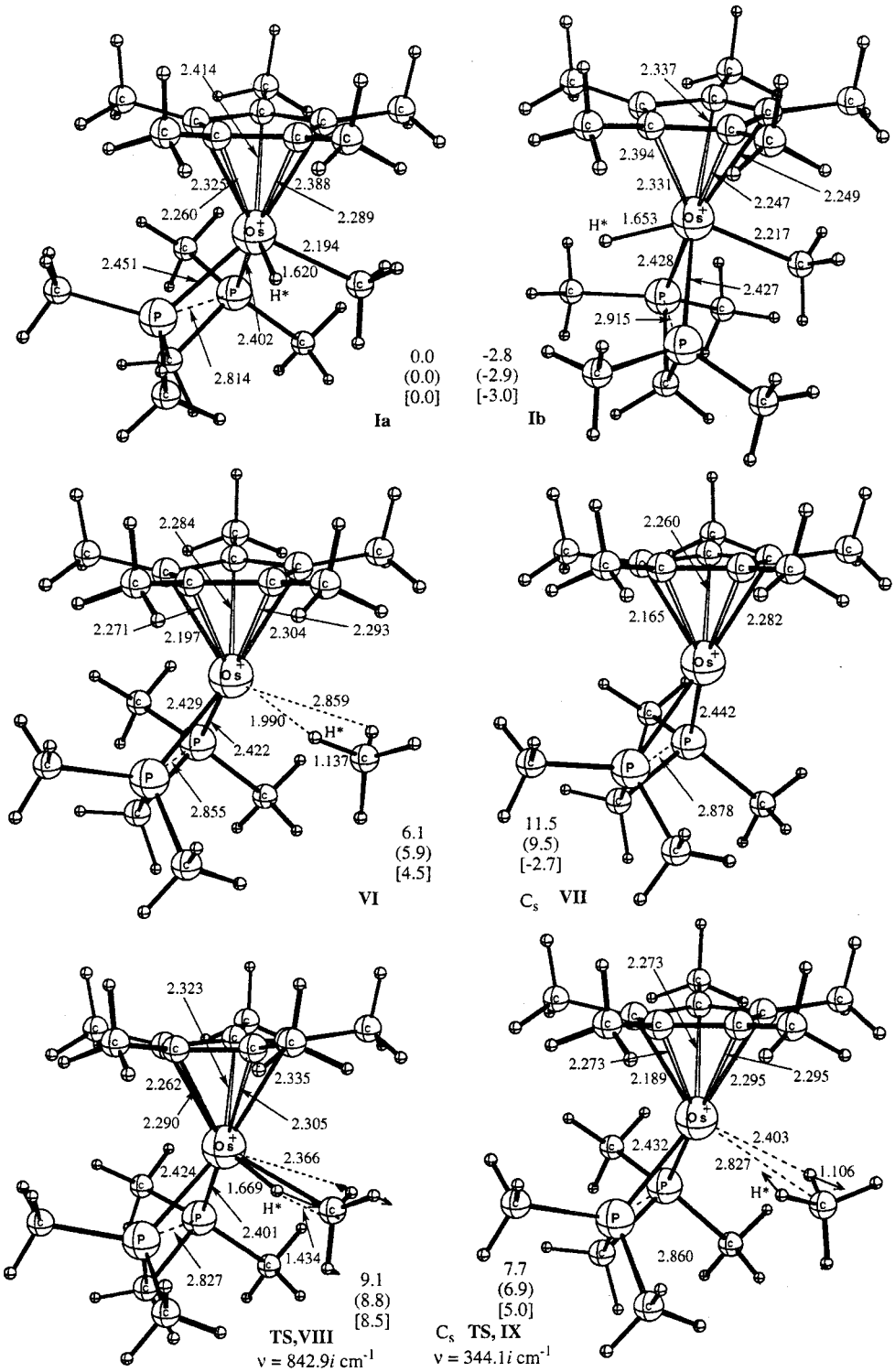

Figure 5. ONIOM optimized structures (distances in Å and angles in deg) and relative energies (ΔE without parentheses, ΔE + ZPC with parentheses, and ΔG in brackets, in kcal/mol relative to **Ia**) of cis (**Ia**) and trans (**Ib**) isomers of the real complex **I**, $[(C_5Me_5)Os(dmpm)CH_3H]^+$, intermediates **VI** and **VII**, and transition states **VIII** and **IX**. For the transition states, the reaction coordinate (denoted by the arrows) and its imaginary frequency are shown.

at the transition state **VIII** with the activation barrier, (ΔE + ZPC) and [ΔG], of (8.8)[8.5] kcal/mol, vs (6.0)-[6.0] kcal/mol in the model system. From the resultant methane complex **VI**, the process may split into two paths, D and E, where path **D** (corresponding to the H-exchange mechanism) looks slightly favorable in (ΔE + ZPC); the largest barrier on path D for the real system is only 2.9 kcal/mol for C−H bond activation at TS **VIII′**. However, in ΔG the associative/dissociative mechanism (path E) becomes competitive with path D.

IV. Conclusions

From the above-presented discussions we can draw the following conclusions.

1. The H-scrambling in the "model" system, [CpOs-$(PH_2CH_2PH_2)(CH_3)H^*]^+$, **1a**, occurs via the H-exchange

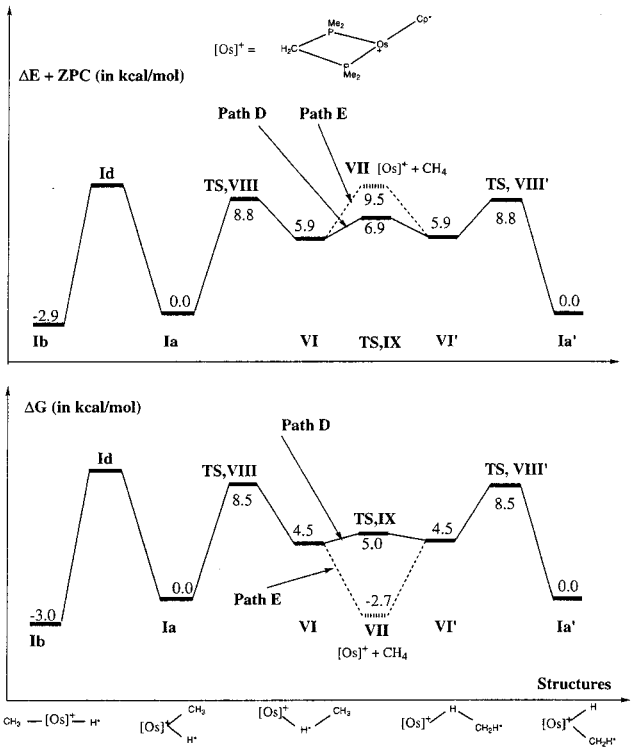

Figure 6. Energy profiles (ΔE + ZPC and ΔG) of H-scrambling in the real complex **Ia** for paths D and E.

mechanism, path D. The first step of the reaction is a C−H* bond formation which occurs with (6.0)[6.0] or (8.9)[8.9]kcal/mol barrier at the transition state **8** in the gas phase and in $CHCl_3$ solution, respectively. Overcoming transition state **8** leads to formation of the methane complex **6**, which is slightly lower in energy than reactant **1a** and where the methane molecule is coordinated to the Os center with its H* atom. Later, complex **6** rearranges to its identical isomer, **6′**, where the methane molecule is coordinated to the Os center with one of its H atoms. The barrier connecting intermediates **6** and **6′** corresponds to the transition state **9** and is calculated to be small, (1.6)[1.6] and (1.5)[1.3] kcal/mol in the gas phase and in $CHCl_3$ solution, respectively. In the next step, the methane C−H bond activation takes place with same type of transition state **8′** as **8** and leads to complex **1a**. The C−H bond activation barrier is found to be (6.2)[7.1] and (7.3)[7.5] kcal/mol in the gas phase and in solution, respectively.

2. Inclusion of the electronic and steric effects from the nine methyl ligands in the calculations, i.e., upon going from the model complex **1a** to the "real" complex **Ia**, did not change our conclusions obtained from the "model" studies, while it destabilized the calculated transition states and intermediates by a few (ca. 3−4) kcal/mol. The rate-determining barrier for the H-scrambling on the "real" system, which again is the C−H* bond formation, increased by 2−3 kcal/mol to (8.8)[8.5] kcal/mol in the gas phase. The calculated C−H bond activation barrier at the TS, **VIII′**, is reduced to (2.9)-[4.0] kcal/mol.

3. The associative/dissociative mechanism corresponding to path E and proceeding via dissociation of the methane molecule from the methane complex **6** (or **VI**) is found to be slightly unfavorable compared to the H-exchange mechanism, path D, at the ΔE + ZPC level both in the gas phase and in solution, but is very close in ΔG (Gibbs free energy). Therefore, the associative/dissociative mechanism may be competitive, especially at higher temperature, to the H-exchange mechanism.

Acknowledgment is made to the Cherry L. Emerson Center of Emory University for the use of its resources, which is in part supported by a National Science Foundation grant (CHE-0079627) and an IBM Shared University Research Award. Computer time allocated at the Center for Supercomputing Applications (NCSA) and Maui High Performance Computer Center (MHPCC) is also acknowledged.

Supporting Information Available: The Cartesian coordinates (in Å) of the optimized geometries of intermediates and transition states for the "model" and "real" systems. This material is available free of charge via the Internet at http://pubs.acs.org.

OM010776O